THE ASTROPHYSICAL JOURNAL, 241: 534–551, 1980 October 15

ON THE SUPERSONIC DYNAMICS OF MAGNETIZED JETS OF THERMAL GAS IN RADIO GALAXIES

K. L. CHAN AND R. N. HENRIKSEN
Astronomy Group, Department of Physics, Queen's University at Kingston, Ontario, Canada
Received 1980 January 25; accepted 1980 April 11

ABSTRACT

A stellar-wind type formulation is developed to study axisymmetric MHD jet flows in radio galaxies. When the magnetic energy is small compared to the total energy of the jet flow and the azimuthal field has a pinching configuration, similarity methods can be employed to reduce the two-dimensional partial differential equations of the problem to a system of ordinary differential equations. These equations allow some approximate analytical solutions in the outer jet region where many parameters approach their asymptotic values, but numerical methods have to be used in the inner jet region where variables change rapidly. The results of the numerical experiments to study the effects of a pinching external pressure and a pinching magnetic field are discussed, and the observed width of the northern radio jet in 3C 449 will be fitted by each of the two pinching models. The asymptotic analytic expressions are tested numerically, and it is shown how they may be used to deduce physical properties of the jet from direct observations of its geometry. In particular, the radius of the jet nozzle, the internal magnetic energy, and the external pressure may be constrained in this manner. The significance of the recently discovered transition from parallel to transverse magnetic field in the jet is also demonstrated.

Subject headings: galaxies: structure — hydromagnetics — radio sources: galaxies

I. INTRODUCTION

Supersonic beams were proposed as a means of transporting energy from intense central sources in galaxies or quasars to distant radio lobes almost a decade ago by Rees (1971). Since then, this idea has been modified and developed extensively (Longair, Ryle, and Scheuer 1973; Scheuer 1974; Blandford and Rees [hereafter BR] 1974; Wiita 1978). In recent years the existence of continuous bridges or jets of radio emission have in some galaxies been confirmed observationally—e.g., NGC 315 (Bridle *et al* 1976), 3C 31 (Burch 1977), NGC 6251 (Waggett, Warner, and Baldwin 1977; Readhead, Cohen, and Blandford 1978). It seems reasonable to assume that the lossy radio jets and the energy beams may be identified, or at least correlated in the sense that the radio electrons act as tracers of the thermal beam.

With the highly sensitive VLA telescope now put into operation, more information about the structure of radio jets has been accumulated (e.g., Bridle *et al*. 1979; Fomalont *et al*. 1980; Perley, Willis, and Scott 1979). In particular, the continuous jets are observed to be highly collimated (usually cone angle $\leq 20°$), and significantly enhanced collimation sometimes develops as the jet goes outward (cone angle decreases). It is also known now that the magnetic fields in these jets are highly organized—for the radiation is polarized (often approaching the theoretical maximum) and the electric vectors are well ordered. Frequently, in one side of the two sided jets,[1] the magnetic field is observed to change its orientation from parallel to perpendicular relative to the jet axis. In view of these observational facts, it is natural to ask the following questions: How can one explain the decrease of cone angle? Does the observed well-ordered magnetic field have dynamically important effects on a radio jet?

Many models proposed to explain radio sources are electrodynamically dominated (e.g., Lovelace 1976; Blandford 1976; Benford 1978). However, in those cases the assumed geometries are usually very restrictive. On the other hand, the popular beam models are hydrodynamical and more flexible in handling the geometry (e.g., Begelman, Rees, and Blandford 1979), but the effects of magnetic fields are usually ignored. In this paper, the dynamical behavior of radio jets is studied by a "transverse self-similar" flow model which incorporates the magnetohydrodynamical effects as well as the usual pressure confinement.

Following the standard treatment in beam models, we shall assume that a "typical" radio jet is continuous, stationary, and that the flow is principally confined and collimated by an external pressure (at least near the central

[1] A. H. Bridle, private communication.

source). However, our formulation will include the possibility of magnetic pinching. Since there is evidence that some jets are nonrelativistic and relatively dense (Perley, Willis, and Scott 1979), we shall make the simplifying assumption that the flow can be described by the nonrelativistic magnetohydrodynamical equations. The magnetic field is assumed to be frozen-in, and the geometry is assumed to be axisymmetric.

We recall that a similar problem has been encountered and studied extensively in connection with magnetized stellar winds (see Weber and Davis 1967; Mestel 1968; Michel 1969; Goldreich and Julian 1970; Henriksen and Rayburn 1971). However, in those cases attention was mainly focused on solutions in the equatorial plane, where analytical results can be obtained. The radio-jet problem is concerned more with flow in the polar directions, and moreover the angular width (θ) of a jet is an important variable which needs to be calculated for comparison with observations.

Thus our present problem is essentially two-dimensional, but fortunately the standard treatment of MHD winds can be nicely generalized to two dimensions (see Appendix A). However, even though this general approach is quite powerful, its application to a completely two-dimensional problem requires the solution of a pair of complicated partial differential equations (e.g., eqs. [A17], [A18]). Fortunately, by assuming paraxial flow, and assuming that the strength of the magnetic field is small and that the dependent variables have self-similar distributions across the flow, it is possible to reduce the partial differential equations to a system of ordinary differential equations which is much easier to solve. Note however that no restrictive self-similarity is required in the z direction.

In § II, the ϖ-similar flow model will be presented (ϖ represents the radial coordinate in a cylindrical system). The properties of these flows as obtained by numerical experiments will be described in § III. Section IV will discuss various implications.

II. THE "ϖ-SIMILAR" MODEL FOR A CONTINOUS JET

A steady MHD flow must satisfy

$$\nabla\times(\mathbf{V}\times\mathbf{B})=\mathbf{0}, \tag{1}$$

$$\nabla\cdot\mathbf{B}=0, \tag{2}$$

$$\nabla\cdot(\rho\mathbf{V})=0, \tag{3}$$

$$\nabla\frac{V^2}{2}+\frac{1}{\rho}\nabla p+\nabla\Phi=\mathbf{V}\times\nabla\times\mathbf{V}-\frac{1}{4\pi\rho}\mathbf{B}\times\nabla\times\mathbf{B}, \tag{4}$$

where Φ is the gravitational potential and all other symbols have their conventional meaning. An equation of state is required to complete the system, and we shall assume that the beam may be treated as an ideal gas ($p\propto\rho T$) and moreover normally that p has a polytropic dependence on ρ, i.e.,

$$p\propto\rho^{\gamma}, \tag{5}$$

along a streamline (γ is a constant). Furthermore, we shall ignore gravitational effects in this paper as we are primarily interested in the outer portions of the jet.

From the streamline formulation discussed in Appendix A, one can obtain the following system of equations in cylindrical coordinates (ϖ, ϕ, z):

$$B_{\varpi}=B_z V_{\varpi}/V_z, \tag{6}$$

$$B_{\phi}=B_z\left(\frac{\varpi\Omega}{V_z}\right)\frac{L/\Omega\varpi^2-1}{1-M_A^{-2}}, \tag{7}$$

$$\left(V_{\varpi}\frac{\partial}{\partial\varpi}+V_z\frac{\partial}{\partial z}\right)B_z=B_{\varpi}\frac{\partial V_z}{\partial\varpi}-B_z\left(\frac{\partial V_{\varpi}}{\partial\varpi}+\frac{V_{\varpi}}{\varpi}\right), \tag{8}$$

$$\left(V_{\varpi}\frac{\partial}{\partial\varpi}+V_z\frac{\partial}{\partial z}\right)\rho=-\rho\left(\frac{V_{\varpi}}{\varpi}+\frac{\partial V_{\varpi}}{\partial\varpi}+\frac{\partial V_z}{\partial z}\right), \tag{9}$$

$$\left(V_{\varpi}\frac{\partial}{\partial\varpi}+V_z\frac{\partial}{\partial z}\right)V_{\varpi}=-\frac{1}{\rho}\frac{\partial}{\partial\varpi}p+\frac{V_{\phi}^2}{\varpi}-\frac{B_{\phi}}{4\pi\rho\varpi}\frac{\partial}{\partial\varpi}(\varpi B_{\phi})+\frac{B_z}{4\pi\rho}\left[\frac{\partial B_{\varpi}}{\partial z}-\frac{\partial B_z}{\partial\varpi}\right], \tag{10}$$

$$V_\phi = (\varpi\Omega)\frac{L/\Omega\varpi^2 - M_A{}^{-2}}{1 - M_A{}^{-2}}, \tag{11}$$

$$\frac{1}{2}(V_\varpi{}^2 + V_\phi^2 + V_z^2) + \int \frac{dp}{\rho} - \frac{B_\phi B_z}{4\pi\rho}\left(\frac{\varpi\Omega}{V_z}\right) = E, \tag{12}$$

where Ω, L (angular momentum per unit mass), and E (total energy per unit mass) are parameters that stay constant along a stream line and

$$M_A = (4\pi\rho V_z^2/B_z^2)^{1/2} \tag{13}$$

is the poloidal Alfvénic Mach number.

We separate the dependencies on ϖ and z by assuming the following ϖ self-similar forms (c.f. Chan, Chau, and Henriksen 1980), namely,

$$\mathbf{B} = \left(b_\varpi \frac{\varpi}{R}, b_\phi \frac{\varpi}{R}, b_z\right), \tag{14}$$

$$\mathbf{V} = \left(W_\varpi \frac{\varpi}{R}, W_\phi \frac{\varpi}{R}, W_z\right), \tag{15}$$

$$L = \Omega R_A{}^2\left(\frac{\varpi}{R}\right)^2, \tag{16}$$

$$T = T_j - (T_j - T_R)(\varpi/R)^2, \tag{17a}$$

where b_ϖ, b_ϕ, b_z, W_ϖ, W_ϕ, W_z, T_j, T_R, and R are functions only of z, and R_A is a constant identified subsequently with R at the Alfvénic point. The scaling radius $R(z)$ is taken to be the radius of the jet boundary at z so that it obeys (boundary is a streamline)

$$dR/dz = W_\varpi/W_z. \tag{18}$$

The quantities T_R, b_ϖ, W_ϖ, etc., are values of T, B_ϖ, V_ϖ, etc., on the boundary streamline, and T_j is the temperature on the jet axis. Moreover, we take ρ to depend only on z as required in Appendix A. Equation (17a) can then be written equivalently as $p = p_j - (p_j - p_R)(\varpi/R)^2$. In general, total pressure balance at $R(z)$ requires

$$p_R = p_e + \frac{B_e{}^2 - B_R{}^2}{8\pi} = p_{Te} - \frac{b_\varpi{}^2 + b_z{}^2}{8\pi} - \frac{b_\phi{}^2}{8\pi},$$

with $p_{Te} \equiv p_e + B_e^2/8\pi$, but we will assume the magnetic field to be strictly continuous at R so that $p_R = p_e$ and so (17a) becomes

$$p = p_j - (p_j - p_e)(\varpi/R)^2. \tag{17b}$$

Here, p_e, the external pressure, is a given function of z, and p_j (a function only of z) will be taken to depend on ρ as in equation (5).

Using equations (15) and (18), the left-hand side of equation (10) becomes

$$\left(V_\varpi \frac{\partial}{\partial\varpi} + V_z \frac{\partial}{\partial z}\right)V_\varpi = \left(\frac{\varpi}{R}\right)W_z \frac{d}{dz} W_\varpi. \tag{19}$$

When equations (14)–(17) and (19) are substituted into equations (6)–(11) and (13), it is found that the assumed ϖ dependencies are indeed compatible with each other, so that relations among the z-dependent functions can be written down without the appearance of ϖ. Furthermore, equations (8) and (9) become integrable. Hence the exactly self-similar relations are:

$$b_\varpi = b_z W_\varpi / W_z, \tag{20}$$

$$b_\phi = b_z\left(\frac{R\Omega}{W_z}\right)\frac{(R_A/R)^2 - 1}{1 - M_A^{-2}}, \tag{21}$$

$$b_z = \Sigma_b / R^2, \tag{22}$$

$$\rho = \Sigma_m / W_z R^2, \tag{23}$$

$$W_z \frac{d}{dz} W_\varpi = \frac{2}{\rho R}(p_j - p_e) + \frac{W_\phi^{\,2}}{R} + \frac{1}{4\pi\rho}\left[b_z R \frac{d}{dz}\left(\frac{b_\varpi}{R}\right) - \frac{2b_\phi^{\,2}}{R}\right], \tag{24}$$

$$W_\phi = (R\Omega)\frac{(R_A/R)^2 - M_A^{-2}}{1 - M_A^{-2}}, \tag{25}$$

where Σ_b and Σ_m, the axial magnetic and material fluxes in the jet, are constants.

However, the assumed forms (14)–(17b) fail to eliminate the ϖ dependence from equation (12), Bernoulli's equation. Using (17a), this becomes explicitly

$$E = \frac{\gamma}{\gamma - 1}\frac{p_j}{\rho} + \frac{W_z^{\,2}}{2} + \frac{\varpi^2}{R^2}\left[\frac{W_\varpi^{\,2}}{2} + \frac{W_\phi^{\,2}}{2} - \frac{b_\phi b_z}{4\pi\rho}\frac{\Omega R}{W_z}\right] + \frac{(p_R - p_j)}{\rho}\frac{\varpi^2}{R^2} + \left[\int \frac{p_R - p_j}{\rho R^2}\frac{d\rho}{\rho}\right]\varpi^2$$

$$\equiv E_z + E_\varpi,$$

where $E_\varpi = \text{const} \times \eta = \text{const} \times [-\rho(W_z/2)\varpi^2]$ and E_z is a constant by Appendix A (E' a constant). Hence the assumed self-similar form overdetermines the problem by yielding two equations from the Bernoulli equation (unless p_j is allowed to be determined by the dynamics rather than eq. [5], or unless an anisotropic pressure is used). We shall avoid this difficulty here by treating the case for which $E_\varpi \ll E_z$ so that Bernoulli's equation reduces to

$$\frac{W_z^{\,2}}{2} + \frac{\gamma}{\gamma - 1}\frac{p_j}{\rho} = E_z. \tag{26}$$

This approximation will be valid provided:

i) $$\frac{|b_\phi b_z|}{4\pi\rho}\frac{\Omega R}{W_z} \ll E_z,$$

ii) $$\frac{W_\varpi^{\,2}}{2}, \frac{W_\phi^{\,2}}{2} \ll E_z$$

and

iii) $$\frac{|p_e - p_j|}{\rho} \ll E_z.$$

Condition (i) requires that the magnetic force be relatively unimportant in accelerating the longitudinal motion of the jet. Note that it *does not* mean that the magnetic forces may be neglected while calculating the *transverse* motion of the jet from equation (24), for the other transverse terms are small in the same order in this approximation.

Condition (ii) is essentially the paraxial stream line approximation $[(dR/dz)^2 = W_\varpi^{\,2}/W_z^{\,2} \ll 1, (Rd\phi/dz)^2 = W_\phi^{\,2}/W_z^{\,2} \ll 1]$. The low rotational velocity is consistent with condition (i), and we note that for a collimation angle of 30°, $(W_\varpi/W_z)^2 \equiv \tan^2 15° \approx 0.07$.

Inasmuch as ∇p_j actually accelerates the jet initially (eq. [26]), condition (iii) must be interpreted as requiring the internal pressure to be very nearly the external pressure when they are large (i.e., near the central source). This is in fact the very condition needed for the Blandford-Rees nozzle to operate. In our numerical experiments (§ III),

$|p_j - p_e|/\rho E_z$ is usually less than a few percent. Only in very unfavorable cases with, say, 20% magnetic or rotational energy can it get as large as 20%, and then only in a small region near the nozzle.

Equations (18) and (20) to (26) now define completely our model in terms of W_z, W_ϖ, b_z, b_ϖ, ρ, R, b_ϕ, W_ϕ ($p_j \propto \rho^\gamma$). In fact, the actual equations to be solved are (18), (24), and (26) for R, W_ϖ, and W_z. We proceed in § III to study these equations numerically, but it is easy to acquire a qualitative appreciation of their behavior.

Looking first at the transverse equation (24), we observe that the magnetic term in b_ϕ is the pure "pinching" term. It is accentuated in our self-similar form by virtue of $B_\phi = b_\phi \varpi / r$ increasing outward. At the same time the repulsive transverse magnetic pressure due to B_z has been set to zero as $B_z = b_z(z)$. The only way we could accommodate this repulsion in our model would be to have B_z discontinuous at $R(z)$, which we do not do here. The other magnetic term in equation (24) is $\sim O[(W_\varpi / W_z)^2 b_z{}^2 / 4\pi\rho R]$ and is therefore normally small compared to the term in b_ϕ^2. Thus the magnetic effects in the model are primarily confining or pinching. The repulsive centrifugal term is related to the strength of the pinching term, however, as b_ϕ and W_ϕ are correlated (eq. [21] and [25]).

The pressure term in equation (24) is normally dominant in the early stages of the jet. As p_e drops along the jet, the jet accelerates and expands. Consequently ρ drops and therefore $p_j (\propto \rho^\gamma)$ declines rapidly. Eventually p_j may become less than p_e (case of confinement), and the jet will be confined radially until once again p_j exceeds or equals p_e. If the amplitude of these oscillations is small enough, the jet will be collimated. For eventually, both p_j and p_e become small, W_ϖ becomes small, and the jet preserves its collimation inertially. On a larger length scale, the secular magnetic pinching term will become important, however.

Equation (26) may be used alone to gain some insight into the longitudinal motion (see Landau and Lifshitz 1959, §§ 80, 90). The standard analysis shows that (here of course the "pipe" cross section is furnished by eqs. [18] and [24] solved simultaneously) the flow is divided into subsonic and supersonic regions by a sonic point at which

$$W_z{}^2 = W_{zs}{}^2 \equiv \gamma (p_j / \rho)_s , \tag{27}$$

and

$$W_{\varpi s} = 0 = W_{zs} (dR/dz)_s . \tag{28}$$

The subscript s is used consistently to denote quantities at the sonic point.

In the subsonic region ($z < z_s$), pressure balance between the "wall" (external gas) and the jet fluid should permit a converging nozzle to form (BR 1974; Wiita 1978; and discussion above). The flow pressure decreases from the central pressure p_c (at $z = 0$) to

$$p_s = \left(\frac{2}{\gamma + 1} \right)^{\gamma/(\gamma - 1)} p_c . \tag{29}$$

However, because of the many possible instabilities (see Blake 1972) which grow rapidly in the subsonic region, this region may be violently turbulent, and one should not take the laminar flow equations (20)–(25) too seriously. Considered as an average, equation (26) may still hold.

Above the sonic point ($z > z_s$), the flow is accelerated in a diverging nozzle. As the nozzle width increases, W_z approaches a limiting value

$$W_{z\infty} = W_{zs} [(\gamma + 1)/(\gamma - 1)]^{1/2} . \tag{30}$$

It is well known (e.g., Blake 1972; Birkhoff and Zarontonello 1957) that the inertial and pressure-driven instabilities are suppressed in such a supersonic jet. (We also expect the surface tension provided by the magnetic field to inhibit Kelvin-Helmholz instability.) The azimuthal magnetic field adds the pinch instability, which in the absence of all other effects would grow spatially (in a supersonic jet the explicit time dependence is dominated by the convective term) as $\sim \exp\{2\varepsilon_B z / R_m\}$ (see Appendix B and § III b below). However, because of the dominance of the convective time dependence at any point, our steady state calculation really itself provides the nonlinear, fundamental mode of the jet. These calculations show that the pinch is stopped by thermal and magnetic pressure and the beam "bounces" on about the above spatial scale. We have not investigated nonaxisymmetric instabilities (e.g., kink and helical modes), but these can be expected to have comparable or slightly larger growth scales. Consequently, in the absence of external disturbances, we feel that our model will be reasonably stable over at least several pinching scales.

Equations (21) and (25) describe the behavior of the azimuthal variables when interactions between the magnetic field and the mechanical angular momentum are included. We observe first that since the flow we are considering has low magnetic energy (i.e., lower than thermal), M_A ($\propto \rho^{-1/2}$) is larger than unity in the supersonic region, so that the supersonic flow is also super-Alfvénic (i.e., $z_A < z_s$ or a "hot" jet). (We shall consider a "cool" jet, $z_A > z_s$, elsewhere.) If M_A becomes equal to unity somewhere inside the subsonic region, the denominators in both equations (21) and (25) vanish. In that case, singularities can be avoided only if $R = R_A$ when $M_A = 1$, and we would be restricted to the critical curve that passes smoothly through R_A. However, this may never happen in reality, since the present ϖ-similar description of the flow certainly breaks down near the central source because of the complicated geometry needed to account for mass and energy conservation there, and it may even break down well above that region due to the existence of serious turbulence in the subsonic region. Thus, we shall normally not have the critical curve restriction on our parameters. It develops, however, that there are physical restrictions on R_A.

We introduce a new parameter

$$R_1 \equiv W_{z\infty}/\Omega, \tag{31}$$

in terms of which equations (21) and (25) can be conveniently written as

$$\frac{b_\phi}{b_z} \approx -\frac{R}{R_1} \quad (R \gg R_A, M_A{}^{-2} \ll 1) \tag{32}$$

and

$$\frac{W_\phi}{W_{z\infty}} \approx \frac{R_A{}^2}{R_1 R} \quad \left(\text{for } M_A{}^{-2} \ll \frac{R_A{}^2}{R^2} \ll 1\right), \tag{33}$$

respectively. The requirement that $M_A{}^{-2} \ll R_A{}^2/R^2$ is essentially that there should be substantial acceleration between z_A and z, which is certainly true if $z_A < z_s$. From equation (32), one can see that $|b_\phi| \approx |b_z|$ when $R = R_1$. This point is therefore close to the location where the transition of the field orientation from parallel to perpendicular takes place, and it can be determined observationally. Since $W_\phi/W_{z\infty}$ in our model must be small everywhere, the following constraint must be imposed on R_A:

$$R_A < (R_1 R_s)^{1/2} \tag{34}$$

(R_s is the minimum radius). Another constraint can be found by arguing that W_ϕ should not change its sign in the flow (at least in the supersonic region where the flow is assumed to be laminar); then a necessary condition is that (using eq. [25])

$$R_A > R_s M_{As}{}^{-1}. \tag{35}$$

In summary, the jet flow can be divided into two regions: an inner region where variables are changing rapidly, and an outer region where asymptotic conditions are reached ($w_z \approx W_{z\infty}$ and eqs. [32], [33] hold). In the outer region, it is possible to describe the jet using some analytical approximations (see Appendix B). However, for the inner region, numerical methods have to be used to solve the full system of differential equations. This is the principal task of the next section, but comparisons will also be made there between the approximate analytical results and numerical results, for the outer region.

III. NUMERICAL CALCULATION OF THE SUPERSONIC REGION

For ease in numerical calculation, equations (20)–(26) are made dimensionless by introducing R_s and W_{zs} as the constant length and velocity scales of the problem. Defining $\mu \equiv W_z/W_{zs}$, $\nu \equiv W_\varpi/W_{zs}$, $\lambda \equiv z/R_s$, $\xi \equiv R/R_s$, $\xi_1 \equiv R_1/R_s$, $\mu_\infty \equiv [(\gamma+1)/(\gamma-1)]^{1/2}$, $f \equiv p_e/p_{es}$, and $\tau \equiv (p_j/p)/(p_j/p)_s$, one can write the three dynamical equations (18), (24), and (26) in the following forms:

$$\mu \frac{d\xi}{d\lambda} = \nu, \tag{36}$$

$$(1 - M_A{}^{-2})\mu \frac{d\nu}{d\lambda} = \frac{1}{\xi}[2p + F_c - 2F_{\phi\phi} - F_{\varpi z}], \tag{37}$$

$$\mu^2 + \frac{2}{\gamma - 1}\tau = \mu_\infty{}^2, \tag{38}$$

where

$$\text{(pressure balance) } P = \frac{\tau}{\gamma} - C_e f(\lambda)\tau^{-1/(\gamma-1)}, \tag{39}$$

$$\text{(centrifugal force) } F_c = \frac{\gamma+1}{\gamma-1}\left(\frac{\xi}{\xi_1}\right)^2\left[\frac{(\xi_A/\xi)^2 - M_A{}^{-2}}{1-M_A{}^{-2}}\right]^2, \tag{40}$$

$$\text{(pinching) } F_{\phi\phi} = \frac{\gamma+1}{\gamma-1}\left(\frac{\xi}{\xi_1}\right)^2 M_A{}^{-2}\left[\frac{(\xi_A/\xi)^2 - 1}{1-M_A{}^{-2}}\right]^2, \tag{41}$$

$$\text{(magnetic surface tension) } F_{\varpi z} = \nu^2 M_A{}^{-2}\left(\frac{3\mu^2-\tau}{\mu^2-\tau}\right), \tag{42}$$

$$\text{(effective temperature) } \tau = (\mu\xi^2)^{(1-\gamma)}, \tag{43}$$

$$M_A{}^{-2} = M_{As}{}^{-2}\xi^{-2}\mu^{-1}, \tag{44}$$

and C_e is an arbitrary constant to be identified with $(p_{es}/\gamma p_{js})$. The $-M_A{}^{-2}$ term on the left-hand side of equation (37) comes from the $F_{\varpi z}$ term in equation (24) (eq. [26] is used). Also note that even though the denominator in the expression for $F_{\varpi z}$ vanishes at the sonic point, ν also vanishes at the sonic point (eq. [28]); therefore $F_{\varpi z}$ actually goes to zero at this point with ν.

In the above system, there are five constant parameters: C_e, γ, M_{As}, ξ_A, ξ_1, and one arbitrary function $f(\lambda)$. By assuming that transverse dynamical balance (i.e., $\mu\, d\nu/d\lambda = 0$) is satisfied at the sonic point, we can set $C_e = 1/\gamma - \frac{1}{2}F_{\varpi z}(S) + \frac{1}{2}F_{cs} - F_{\phi\phi}(S)$ since $\tau_s, f_s = 1$ by definition which gives $C_e(\gamma, M_{As}, \xi_A, \xi_1)$. In our numerical experiments, γ is fixed to be 4/3 (radiation-like) while the form of $f(\lambda)$ is restricted to be

$$f(\lambda) = f_1/\left[1 + (\lambda/\lambda_s)^m (f_1 - 1)\right] \quad \text{(power law)} \tag{45a}$$

$$= f_1 \exp\left[-(\ln f_1)\left(\frac{\lambda}{\lambda_s}\right)^2\right] \quad \text{(Gaussian)}, \tag{45b}$$

where $f_1 = [(\gamma+1)/2]^{\gamma/(\gamma-1)}$ [see eq. (29) and note that $f_1 = f(\lambda=0) = f_c$; transverse pressure balance at $\lambda < \lambda_s$ is also assumed], m is the exponent for a power law distribution of the external gas pressure, and λ_s ($\equiv z_s/R_s$) is *another free parameter* which specifies the distance of the sonic point from the center. Since $F_c \propto \xi^{-2}$ and $F_{\phi\phi} \approx [(\gamma+1)/(\gamma-1)]$ $(M_A\xi_1/\xi)^{-2} \approx$ constant in the outer jet region, $F_{\phi\phi}$ is secularly much more important than F_c. Similarly, the terms $-M_A^{-2}$ and $F_{\varpi z}$ are not very important in (37) compared to $F_{\phi\phi}$. Noting equation (44), we may observe that M_{As} and ξ_1 appear in the form $(M_{As}\xi_1)^{-2}$ in the asymptotic expression for $F_{\phi\phi}$, and thus one can replace them by a single parameter,

$$\epsilon_B \equiv \mu_\infty^{-1}(M_{As}\xi_1)^{-2} \approx \frac{b_\phi{}^2}{4\pi\rho W_{z\infty}{}^2}, \tag{46}$$

which has the physical meaning of being the ratio of magnetic energy to kinetic energy in the outer jet region. Therefore, aside from the freedom in the external pressure distribution, the problem is *essentially* determined by a single parameter ϵ_B and we have made use of this numerically. (Some cases with M_A and ξ_1 varying and ϵ_B fixed have been calculated to test this statement; the perturbations in the results are small for $\epsilon_B < 2\%$.) In the asymptotic jet region where both p_j and p_e are negligible, an analytic solution can be found which depends only on ϵ_B (Appendix B).

To restrict our parameter space for this paper we set $M_{As}{}^{-2}$ arbitrarily as $[2/(\gamma+1)]^{1/(\gamma-1)} \approx 0.63$. Inasmuch as equation (29) may be written as (recall, e.g., [A16]) $M_{As}{}^{-2} = [2/(\gamma+1)]^{1/\gamma-1} M_{Ac}{}^{-2}$, and recalling that our assumed form will not continue to the actual center, this choice allows M_A to become $\lesssim$ in the subsonic region, as is physically likely. Equations (34) and (35) now become $R_A/R_s < \xi^{1/2}$ and $R_A/R_s > 0.79$, respectively, the first of which is $R_A/R_s < M_{As}{}^{-\frac{1}{2}}\mu_\infty{}^{-\frac{1}{4}}\epsilon_B{}^{-\frac{1}{4}} \sim \epsilon_B{}^{-\frac{1}{4}} \sim 3.2$ for $\epsilon_B \sim 1\%$. We see therefore that $\xi_A \equiv R_A/R_s$ is constrained to be $O(1)$, and we fixed it to be 1 in the calculations. This leaves us only ϵ_B(i.e., ξ_1), λ_s and any other parameters introduced through $f(\lambda)$ to vary. We consider the following particular cases.

TABLE 1

ASYMPTOTIC CONE ANGLES WITH **B**=0

m	λ_s = 5	10	30	90
$m=3$	21, 7.6(2)	13, 5.2(3)	5, 4.2(4)	...
$m=4$	...	31, 6.5(2)	18, 5.6(3)	10, 3.5(4)
$m=5$	...	41, 2.0(2)	27, 1.4(3)	17, 7.8(3)
$m=6$	...	47, 1.0(2)	33, 5.8(2)	22, 3.2(3)
Gaussian ...	...	53, 7.2(1)	43, 2.2(1)	36, 6.7(2)

TABLE 2

RESULTS OF PINCHING BY EXTERNAL PRESSURE

	$m=4, \lambda_s=20$			$m=5, \lambda_s=30$			$m=6, \lambda_s=40$		
Parameter	300[a]	1500[a]	9000[a]	300[a]	1500[a]	9000[a]	300[a]	1500[a]	9000[a]
λ_t	2.3(2)	1.8(3)	2.4(4)	2.8(2)	3.2(3)	8.5(4)	4.1(2)	8.3(3)	4.2(5)
ξ_t	1.6(1)	2.6(2)	4.3(3)	2.5(1)	6.5(2)	2.0(4)	5.1(1)	2.0(3)	1.1(5)
$(d\xi/d\lambda)_t$...	0.09	0.16	0.19	0.13	0.22	0.24	0.19	0.26	0.27
$\lambda_{\max_1}$	5.3(2)	8.4(3)	3.1(5)	6.7(2)	2.6(4)	2.3(6)	1.1(3)	1.0(5)	2.2(7)
$\xi_{\max_1}$	3.4(1)	9.4(2)	3.5(4)	5.8(1)	3.8(3)	3.4(5)	1.3(2)	1.8(4)	3.9(6)
ξ_t^*	2.2(1)	4.0(2)	4.3(3)	4.0(1)	9.2(2)	2.1(4)	3.0(1)	2.0(3)	1.3(5)
f_e	4.3(−5)	6.9(−8)	5.3(−11)	2.2(−5)	6.9(−9)	8.9(−13)	6.1(−6)	3.9(−10)	8.4(−14)
f_e^*	1.7(−4)	9.9(−8)	5.6(−11)	5.1(−5)	8.6(−9)	9.3(−13)	7.6(−6)	4.3(−10)	9.8(−15)

[a] λ_e.

a) No Magnetic Pinching

If $\epsilon_B \to 0$ or if $\boldsymbol{B}$ has a force-free configuration, then $F_{\phi\phi}$, $F_{\varpi z}$, M_A^{-2} can be set to zero, and F_c can also be taken small (rotation generates b_ϕ). Then the transverse behavior of the jet depends only on the variation of the external pressure with z. Asymptotically, the problem can be treated analytically for constant p_e (Appendix B), but we present the numerical integration here.

For simple p_e distributions (eqs. 45a, b]), the instantaneous cone angle 2 $\tan^{-1}(d\xi/d\lambda)$ of a jet increases monotonically in the inner region and approaches a constant asymptotic value in the outer jet region. In Table 1, the first number in each slot is the asymptotic cone angle in degrees and the second number gives the distance λ_{asym} at which $d\xi/d\lambda$ reaches 90% of its asymptotic value. We find λ_{asym} is larger the slower the drop in the external pressure. Moreover, the smaller the required opening angle, the longer the scale length in p_e must be. From this table, one can see that to produce jets with very small cone angles (say $<5°$) by pressure confinement alone requires unrealistically extreme extensions of the atmosphere beyond the sonic point. Indeed for such small angles, p_e must not drop faster than λ^{-3} in a region $\sim 10^3$ times the length of the subsonic region. The asymptotic cone angles produced by Gaussian variations of external pressure are usually too large for reasonable z_s/R_s ratios.

Next, the possibility of subsequently reducing the cone angle by flattening the pressure distribution in the outer region is studied. Numerically, a term of the form $g(\lambda)=[(\lambda-\lambda_s)/\lambda](f_2/\lambda^{m'})$, where $m'<m$, is added to equation (45a). In this expression, $f_2=[f_1/(f_1-1)](\lambda_s/\lambda_e)^m \lambda_e^{m'}$, where λ_e is a length which specifies the location at which $g(\lambda_e) \approx f(\lambda_e)$ (i.e., the location of the break in the power-law external pressure distribution). It was found that if $\lambda_e > \lambda_{\text{asym}}$ and $m'>2.5$, the effects due to a break in the external pressure distribution are extremely small (independent of the initial m). This fact can be readily understood by inspecting the expression for P. For confinement will occur only if $P<0$ beyond $\lambda_e > \lambda_{\text{asym}}$. But $f(\lambda) \propto \lambda^{-m'}$ here, and $\tau \propto \xi^{-2(\gamma-1)} \propto \lambda^{-2(\gamma-1)}$, so that the first term in (39) varies as $\lambda^{-2\gamma+m'}$ times the magnitude of the second (negative) term. Therefore, only if $m'<2\gamma=8/3$, can the negative part of P come to dominate at large λ.

In the case where such external pressure pinching *is* effective, $d\xi/d\lambda$ starts decreasing when the jet reaches λ_e; sometimes it becomes negative. Table 2 summarizes the results of some cases with $m'=0$; the subscript t is used to denote quantities at the location where $d^2\xi/d\lambda^2=0$ ($d^2\xi/d\lambda^2$ changes from >0 to <0), and the subscript "maxi" is used to denote quantities at the location where ξ reaches its first maximum ($d\xi/d\lambda=0$ at this point). After this point the jet width recollapses and will undergo a series of periodic oscillations similar to the one depicted in curve (a) of Figure 1. These oscillations are characteristic of $m'<2\gamma$, and will not occur otherwise.

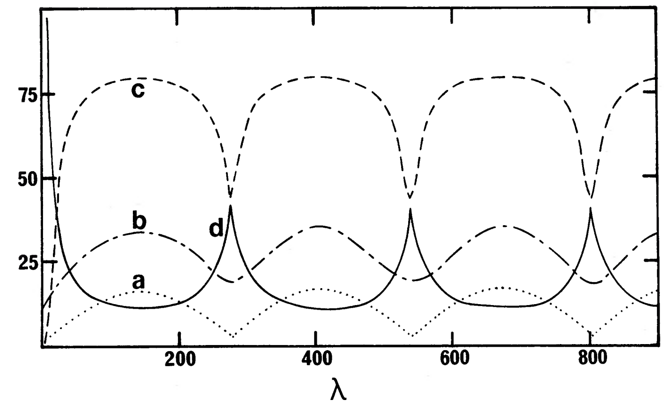

FIG. 1.—Typical behavior of a magnetically pinched jet: (a) ξ; (b) $(\gamma-1)\,|\mathbf{b}|^2/(8\pi p_j)$ in percent; (c) $\tan^{-1}(b_\phi/b_z)$ in degrees; (d) τ in percent. The parameters are $\lambda_j=8$, $\xi_1=3.2$ ($\epsilon_B\sim 2.3\%$), $m=6$, $\xi_A=1$, and $M_{AS}^{-2}=0.63$.

Since $f(\lambda)$ approaches a constant (plateau in p_e) as λ becomes larger than λ_e, the behavior of the jet in this region can be described by the analytical approximation discussed in Appendix B. In Table 2, the values of ξ_t^* and f_e^* as computed by equations (B8) and (B5) are tabulated for comparison. One can see that the agreement is quite good, especially for larger values of λ_t, as the residual effects of the initial external pressure (eq. [45a]) become smaller. The possible applications of equations (B5) and (B8) will be discussed in § IV.

b) *Magnetic Pinching*

If $F_{\phi\phi}\neq 0$, the pinching effect will eventually be able to recollapse the jet width no matter how small ϵ_B is (see Appendix B). The typical behavior of a magnetically pinched jet is depicted in Figure 1. Curves a, b, c, and d plot respectively ξ, $(\gamma-1)|\boldsymbol{b}|^2/(8\pi p_j)$, $\tan^{-1}(b_\phi/b_z)$, and τ versus λ; for a case with $\lambda_s=8$, $\xi_1=3.2$ ($\epsilon_B\sim 2.3\%$), $m=6$, $\xi_A=1$, and $M_{A_s}^{-2}=0.63$. Many similar cases with different parameters have been examined, and the following general properties have been observed: (i) The jet undergoes quasi-periodic oscillations in which the magnetic force and the internal pressure dominate in turn. At the nodes in the jet width, peaks in τ occur. The average width of the jet stays almost constant (in fact, a very small increase in amplitude and period exists from period to period) so that the averaged jet behaves like a tunnel and the adiabatic losses are avoided. The presence of a shoulder in the external pressure variation together with the appropriate parameter choices can cause the amplitude of the oscillation to be smaller than the indicated in Figure 1 (and in Fig. 2b). (ii) The ratio of the organized field energy to the internal energy oscillates generally through a few tens of percent near unity but can reach an order of magnitude in amplitude when $\epsilon_B<0.2\%$. Observationally,[2] polarization percentages (sensitive to the organized field component) oscillate through a few tens of percent near 50%. Thus lower limits may be set for ϵ_B (few %), and quasi-equipartition probably applies in such jets if the internal pressure is largely due to relativistic particles. (iii) Starting with a value less than 45°, $\tan^{-1}(b_\phi/b_z)$ increases above 45° and subsequently oscillates but normally stays above 45° (observed $\boldsymbol{B}$ vector changes from parallel to perpendicular to the jet axis, but it does not subsequently revert to the parallel direction except possible at the nodes). The distance z, at which this transition occurs, is one of the quantities fitted to the observations. These properties are illustrated in Figure 1.

Moreover, in Appendix B, we show that, when only magnetic pinching operates ("cold" jet),

$$\epsilon_B=\frac{1}{4}\pi\alpha^2, \tag{47}$$

where $\alpha\equiv R_{\max}/(z_{\max}-z_{\min})$, the jet radius at maxima divided by the semiperiod, where a period is from node to node or antinode to antinode. Table 3 lists the actual ϵ_B/α^2 found in various cases (including pressure and other nonmagnetic effects), and it is approximately constant. Empirically, the constant to be used in (47) is closer to 2, but decreases as λ_t increases.

[2]A. H. Bridle, private communication

TABLE 3

RESULTS OF PINCHING BY MAGNETIC FIELD

	$m=3, \lambda_s=5$			$m=5, \lambda_s=30$			Gaussian $\lambda_s=30$		
Parameter	3[a]	5[a]	10[a]	3[a]	5[a]	10[a]	3[a]	5[a]	10[a]
λ_t..........	9.3(0)	2.5(1)	1.9(2)	6.3(1)	1.8(2)	1.1(3)	1.1(2)	1.7(2)	6.1(2)
ξ_t..........	1.2(0)	2.7(0)	2.5(1)	1.7(0)	9.5(0)	1.5(2)	4.6(0)	1.9(1)	1.7(2)
$(d\xi/d\lambda)_t$....	0.08	0.11	0.13	0.05	0.08	0.16	0.09	0.23	0.34
$\lambda_{\max_1}$.......	2.3(2)	6.0(2)	4.1(4)	2.2(2)	7.9(2)	1.9(5)	1.7(2)	2.9(3)	2.0(9)
$\xi_{\max_1}$.......	5.2(0)	3.0(1)	2.0(3)	5.1(0)	3.5(1)	1.0(4)	7.5(0)	2.8(2)	1.1(8)
Period......	1.1(2)	1.1(3)	8.8(4)	1.1(2)	1.2(3)	5.0(5)	1.4(2)	7.4(3)	4.0(9)
α...........	0.093	0.055	0.045	0.093	0.058	0.040	0.107	0.076	0.055
ϵ_B/α^2.......	3.1	3.1	1.2	2.8	2.8	1.5	2.3	1.6	0.79

[a] ξ_1.

c) *An Example*

To demonstrate how the present model of jet flows can be applied specifically, a case study on the northern jet of 3C 449 is presented here. Recent observations have made available some detailed information on the structure of this jet (see Perley, Willis, and Scott 1979 and references therein). For simplicity, we assume that the jet axis is perpendicular to the line of sight. This may well be wrong, but our purpose here is only to illustrate the application of the model.

In Figure 2, the developement of the jet width is fitted by two models. For curve (a), the forms related to the magnetic field are suppressed in equation (37) but an extra term of the form $[(\lambda-\lambda_s)/\lambda]f_3/[1+(\lambda/H)^{m'}]$ is added to equation (45a) to create a shoulder in the external pressure distribution $[f_3 \equiv (\lambda_s/\lambda_e)^m f_1/(f_1-1)]$. The fitted values of the parameters are: $m=5$, $m'=3$, $\lambda_s=15$, $\lambda_e=105$, and $H=200$, corresponding to ($H_0=70$ km s^{-1} Mpc^{-1}), $R_s \approx 0.058''$ (20 pc), $Z_s=0.87''$ (300 pc), $z_e \approx 6''$ (2 kpc), and $H \sim 12''$ (4 kpc).

It turns out that the development of the jet width can also be fitted by a magnetic pinching model as in curve (b). For this model, the values of the parameters are: $m=5$, $\lambda_s=12$, $\xi_1=5$, and $\epsilon_B \sim 1\%$, corresponding to $R_s \approx 0''.035$ (12 pc) and $z_s \approx 0''.42$ (140 pc). The point where $b_\phi = b_z$ is located at $\lambda_1=45$ ($\approx 1''.6$) and has not been observed in this source. Fits of this type with the shoulder term can reduce the subsequent oscillations in amplitude.

IV. DISCUSSION

In this paper, we have outlined a rather general method for treating MHD "jet" flows. In § II, however, we restricted our detailed discussion to the "transverse" or ϖ self-similar model. This model requires for its justification a number of physical restrictions that we have already discussed, but we comment here on the choice of the transverse self-similarity itself.

By setting $\rho=\rho(z)$, we are assuming transverse "incompressibility" at least at some initial cross-section. The forms assumed in equations (14), (15) are just such as to be consistent with this transverse incompressiblity, for they imply that a poloidal field-line or streamline is given by the equation $\varpi(z)=\text{const.}\times R(z)$ (where the constant labels a

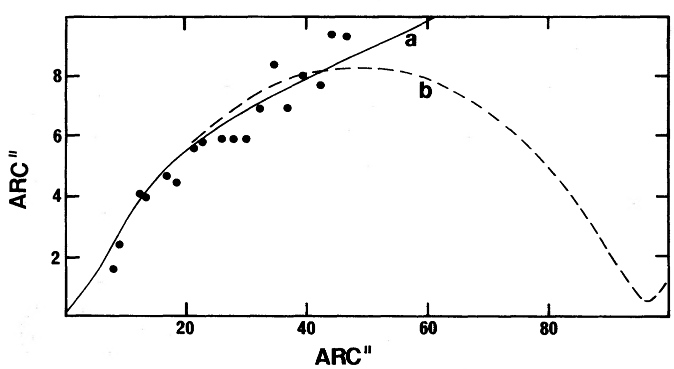

FIG. 2.—Fits for the northern jet of 3C 449: vertical, jet width in arcsec; horizontal, distance along the jet axis.

given streamline). This therefore permits radially only a homologous dilation or compression with the jet boundary, which is consistent with $\rho=\rho(z)$ provided ρ is independent of radius at some initial cross section. The parabolic temperature or pressure profile assumed in equation (17) is also the only variation consistent with transverse incompressiblity, as it prevents the streamline label from appearing in the transverse equation of motion, (37). The choice (16) is the only one that maintains the homologous form for B_ϕ and V_ϕ, while allowing their mutual interaction. We emphasize that the form of the longitudinal variations is not restricted except by the equations themselves.

Physically, the local transverse "incompressibility" should not be too unrealistic at any cross section if magnetosonic waves can traverse the beam diameter in a time, R/W_{ms}, short compared to z/W_z, at that cross section. This amounts to $(W_z/W_{ms})(R/z)\ll 1$, which again holds for a well collimated "paraxial" or "jetlike" flow in the subsonic region and inner supersonic region. Once such transverse self-similarity is established at any section, it can propagate itself in z.

The form for the magnetic field (14) also propagates itself in z with the flow (this statement is in fact what we mean when we say that the steady MHD equation admits the self-similar form [14]). We need only assure ourselves that such a field distribution can arise naturally at some cross section before the onset of the steady state. Thus consider, for example, the radially confined ($V_\varpi=0$) uniformly rotating, hot "atmosphere" of a magnetic dipole spinar. Then near the axis at $t=0$, $B_\varpi\propto\varpi/z^4$; $B_z\propto 1/z^3$, and moreover $B_z(z,t)$, $V_z(z,t)$, $B_\phi\propto\varpi b_\phi(z,t)$, $B_\varpi\propto\varpi b_\varpi(z,t)$, $V_\phi\propto\Omega(z,t)\varpi$ are self-similar forms of the *time-dependent* MHD equation. Thus they can arise naturally in the transition to an eventual steady state from the initial dipole atmosphere.

In § III and with the asymptotic form of Appendix B, we have presented our specific conclusions. When the magnetic field is not dynamically important ($\epsilon_B\to 0$), the result of Table 1 apply. We can conclude that a single power-law external pressure can produce the very small cone angles (5°–10°) observed in some sources only if it does not decline more rapidly than λ^{-3} over $\sim 10^3$ times the length of the subsonic region. A single Gaussian component is quite unable to produce such small cone angles for any reasonable values of λ_s (when λ_s is large, the subsonic region is more likely to be unstable). Table 1 thus summarizes neatly the collimation ability of a smoothly varying external pressure in the post-nozzle region.

Table 2 summarizes our results when the external pressure was taken to have two power-law components, together producing a transition to the flatter law at λ_e. We found that with *sufficiently flat* outer regions the cone angle declines and even becomes negative (the beam reconverges), which leads to a series of oscillations as discussed in Appendix B and illustrated in Figure 1*a*. For steeper outer pressure laws the oscillations degenerate to the "one swing" case of Table 1 and curve (*a*) of Figure 2.

When $\epsilon_B=0$ *and the external pressure is asymptotically flat* (e.g., extended halo or cluster atmosphere), we have found some relations in Appendix B which should allow ready estimates of R_s and p_e (f_e) from simple geometrical observations. Thus from (B8) ([B7] if $\gamma\neq 4/3$) we have

$$\frac{R_t}{R_s}\approx(0.061)\left[\frac{(R_m/R_t)^2-4}{(dR/dz)_t^2}\right]^{3/2}.$$

Consequently, observing R_m, R_t, and $(dR/dz)_t$ will yield R_s, the scale of the sonic nozzle. Equation (B5) then gives f_e as 0.273 $(R_t/R_s)^{-8/3}=p_e/p_{js}$. From Table 2, one can see that a very small value of f_e can pinch the jet. Finally (B9) yields

$$R_n=5.2(R_t/R_m)^3R_t,$$

as a prediction or as a consistency check if R_n is observed.

The magnetic field continues to be given by equations (20)–(22) even when dynamically weak, and in particular equations (31) and (32) apply in the appropriate regime. The quantities R_1 and z_1 are directly observable in some sources (allowing for projection effects) and together define a cone angle that must be fitted by the model. With $\xi_1\equiv R_1/R_s$ determined, equation (46) gives an upper limit for ϵ_B:

$$\epsilon_B=\mu_\infty^{-1}M_{As}^{-2}\xi_1^{-2}<0.238\left(\frac{R_s}{R_1}\right)^2\quad(\gamma=4/3,\, M_{As}^{-2}\leq 0.63).$$

We note also that oscillations in R must produce oscillations in the pitch angle of the field by (32), so that this type of variation shown in Figure 1 is not peculiar to the case where the magnetic field is dynamically important. However, as we have already remarked, this requires an unrealistically flat outer pressure variation ($m'<2\gamma$).

When the magnetic field is dynamically important (ϵ_B at the few % level), Table 3 applies. Although the external pressure was supposed to have the simple power law form of equation (45a) throughout these calculations, such beams always oscillate (Appendix B), and the period is given in Table 3. When ξ_{A} and $M_{\mathrm{A}s}$ are fixed by the approximate considerations given in the text, the only arbitrary parameters occurring are ϵ_B, λ_s, and m (the pressure power law). Figure 1 illustrates the general behavior for such a beam. The oscillations in radius, position angle, and internal energy are clear. It is noteworthy that the magnetic energy is within a factor 3–4 of the internal thermal energy in this regime, and this factor is not very different from that in the fitted region of 3C 449 (Fig. 2). Adiabatic losses are minimized (except on initial expansion) by the averaged cylindircal character of the oscillating beam.

When the general behavior is adequately fitted by a magnetically pinched beam, Appendix B supplies some simple relations analogous to those of the pressure case above. First, the approximate value of ϵ_B can be estimated by equation (47) when R_m and the half-period are determined. Then, with equation (B6), the size of the sonic radius can be estimated by

$$R_s \approx 47 \epsilon_B{}^{3/2} R_t,$$

while (B12) is

$$R_n/R_s \approx 0.04/[\epsilon_B \ln(R_m/R_n)]^{3/2}$$

which may be used to test consistency. When in addition R_1 is observed, then by (46)

$$M_{\mathrm{A}s}{}^{-2} \approx 2.65 \epsilon_B R_1{}^2/R_s{}^2,$$

which may be tested by the model fit (varying $M_{\mathrm{A}s}$). However, we remark that the above estimates are very inaccurate in a region where the external pressure is still significant (as in the examples of Table 3).

We may note that the magnetic fit to the "first swing" of 3C 449 requires $\epsilon_B \approx 10^{-2}$. Taking (Perley, Willis, and Scott 1979) $n_i \approx 0.02$ cm^{-3}, $W_{z\infty} \sim 1000$ km s^{-1} with this ϵ_B yields $b_\phi \approx 6$ microgauss, which value is not untypical of the "equipartition" fields in this source. Our point, however, is that this strength of magnetic field is already dynamically significant. Should magnetic pinching be definitely not observed despite ordered fields of this strength, then we must conclude either that (i) the gas density and/or its velocity are significantly larger than those estimated by Perley, Willis, and Scott (1979), (ii) B_ϕ does not have a pinching configuration, or (iii) significant deviations from the ρ^γ law for the internal pressure occur. This latest possibility is consistent with other indications of internal "heating" or particle reacceleration. We suggest below that such heating may occur in a "core-jet" along the axis of the visible beam.

Once again we note that a combination of an external pressure shoulder with magnetic pinching can remove the violent oscillations. The previous analysis (for $p_e = 0$) does not apply to this case, and full calculations must be done.

It appears[3] that the field transition point will be readily observable in some sources; and may show an important systematic variation. Thus, let us recall that $\Omega R_1 \equiv W_{z\infty}$. Using equation (26) of the text, we may write this as

$$\Omega R_1 = \left(\frac{2}{\gamma - 1}\right)^{1/2} W_c \sim T_c{}^{1/2}, \tag{48}$$

where W_c is the central sound speed and T_c is the central temperature. If Ω does not vary much from object to object [$\Omega \sim (G\bar{\rho}_c)^{1/2}$ on simple-minded arguments], then R_1 will vary as the square root of the central temperature. However, the radiated intensity from an optically thick relativistic Maxwellian distribution of electrons [$N_0 E^2 e^{-E/kT} = N(E)$; e.g., Pacholczyk 1970] is proportional to T. Hence we may expect (ω is a frequency at which the core is optically thick) the length of the parallel field region to be

$$z_1 \equiv (\cot\theta_1) R_1 \quad S_\omega{}^{1/2} \cot\theta_1. \tag{49}$$

Thus, if the cone angle is constant from source to source, we expect $z_1 \propto S_\omega{}^{0.5}$ (core). If, however (as might be expected if the beam cools rapidly beyond the nozzle), $\tan\theta_1 \propto 1/W_{z\infty} \propto T^{-0.5} \propto S_\omega{}^{-0.5}$, then $z_1 \propto S_\omega{}^{1.0}$ (core). This expected correlation can be checked observationally.

[3]A. H. Bridle, private communication.

In a source such as 3C 449 an additional puzzle arises. Fits to the observed jets (either with $\epsilon_B=0$ and external pressure pinching, or with ϵ_B at the few percent level) tend to suggest that the sonic point occurs on a scale of order 100 pc. However, VLBI observations have shown that in at least one case (e.g., NGC 6251, Readhead, Cohen, and Blandford 1978) collinear jetlike structures exist on parsec scales contemporaneously with the large-scale jets we have discussed in this paper. How can there be a causal relation between jets that must have nozzles of such different scales? We propose that in fact small-scale jets can initiate jets on a larger scale by the heating and entrainment of material which surrounds them. Thus, a sub-parsec scale jet may heat surrounding material on, say, a 10 pc scale, which then nozzles through cooler surrounding material and repeats the procedure on the next scale. The actual size of the steps will depend on the scale height of the cool pinching material. In this way, there may actually be many layers to a jet (various layers could stop at different distances however).

Such a structure certainly cannot be described by our ϖ similar model. The simplest modification is to treat the jet as a "two-level" structure, the outer, observed, beam requiring only pressure confinement while the inner, so far unobserved, level might have magnetic confinement. This axial jet could serve as a conduit for high energy particles, or it may produce them in the course of the various pinches it will undergo. Such a picture suggests that relativistic particles may diffuse from the axis of the large-scale beam. Thus, it may be worth making careful observations of the transverse variation in spectral index, position angle and polarization as a test of this "multilevel" concept.

This work was supported by an operating grant from the Natural Science and Engineering Research Council of Canada, and by various grants from Queen's University. The authors acknowledge valuable conversations with Dr. J. P. Vallée and Professor A. H. Bridle of the Queen's Astronomy Group and with Dr. G. V. Bicknell, now at Canberra. They also wish to thank Mrs. Brynn Green for her superb rendering of an impossible manuscript.

APPENDIX A

STREAMLINE FORMULATION FOR AXISYMMETRIC, ROTATING, STATIONARY, MHD FLOWS

The present derivation is a generalization of the classical results in magnetized stellar winds and some of the arguments are closely parallel to those in standard treatments of this problem (e.g., Weber and Davis 1967; Mestel 1968). The readers are referred to those papers for more detailed physical explanations.

The basic equations are equations (1)–(5) in § II. Because of axial symmetry, it is convenient to decompose a vector into two components: the poloidal component which lies in a plane passing through the axis of symmetry, and the azimuthal component which is perpendicular to this plane. Therefore, we write

$$\mathbf{B}=\mathbf{B}_p+\mathbf{B}_\phi, \tag{A1}$$

$$\mathbf{V}=\mathbf{V}_p+\mathbf{V}_\phi, \tag{A2}$$

where the subscripts p and ϕ denote "poloidal" and "azimuthal," respectively. The relations $\boldsymbol{B}_p\cdot\boldsymbol{B}_\phi=\boldsymbol{B}_p\times\boldsymbol{B}_p=\boldsymbol{B}_\phi\times\nabla\times\boldsymbol{B}_p=\mathbf{0}$ (also true for $\mathbf{V}$) will prove to be useful in deriving the formulae below.

In cylindrical coordinates, the two continuity equations (eqs. [2] and [3]) can be satisfied by defining two functions η and A which satisfy

$$\rho\varpi V_\varpi=\frac{\partial\eta}{\partial z}, \tag{A3}$$

$$\varpi\rho V_z=-\frac{\partial\eta}{\partial\varpi}, \tag{A4}$$

$$\varpi B_\varpi=\frac{\partial A}{\partial z}, \tag{A5}$$

$$\varpi B_z=-\frac{\partial A}{\partial\varpi}, \tag{A6}$$

The above equations immediately yield $\boldsymbol{V}_p\cdot\nabla\eta=0$ and $\boldsymbol{B}_p\cdot\nabla A=0$, so that η and A label poloidal streamlines and field lines, respectively. The frozen field condition (eq. [1]) implies that $\boldsymbol{V}\times\boldsymbol{B}=\nabla\psi$, where ψ can be identified as the electric potential ($\boldsymbol{E}=-\nabla\psi$), and this expression can be expanded to read

$$\frac{1}{\varpi^2\rho}\left(\frac{\partial\eta}{\partial z}\frac{\partial A}{\partial\varpi}-\frac{\partial\eta}{\partial\varpi}\frac{\partial A}{\partial z}\right)=\frac{1}{\varpi}\frac{\partial\psi}{\partial\phi}, \tag{A7}$$

$$-\frac{V_\phi}{\varpi}\frac{\partial A}{\partial\varpi}+\frac{B_\phi}{\varpi\rho}\frac{\partial\eta}{\partial\varpi}=\frac{\partial\psi}{\partial\varpi}, \tag{A8}$$

$$-\frac{V_\phi}{\varpi}\frac{\partial A}{\partial z}+\frac{B_\phi}{\varpi\rho}\frac{\partial\eta}{\partial z}=\frac{\partial\psi}{\partial z}. \tag{A9}$$

Equations (A8) and (A9) combine to yield

$$\frac{\partial\eta}{\partial z}\frac{\partial\psi}{\partial\varpi}-\frac{\partial\eta}{\partial\varpi}\frac{\partial\psi}{\partial z}=-\rho V_\phi\frac{\partial\psi}{\partial\phi}. \tag{A10}$$

Consequently, if $\partial\psi/\partial\phi=0$ [i.e., no azimuthal emf, which would be strictly inconsistent with the stationary state ($\nabla\times\boldsymbol{E}=\boldsymbol{0}$) unless there are local batteries], equation (A7) implies that $A=A(\eta)$ so that the poloidal field lines and stream lines are parallel:

$$\mathbf{B}_p=\rho A'\mathbf{V}_p. \tag{A11}$$

(In this Appendix, a prime is used to denote differentiation with respect to η.) Similarly, equation (A10) implies that $\psi=\psi(\eta)$ so that the electric vector $\boldsymbol{E}=-\psi'\nabla\eta$ is *perpendicular to the poloidal field lines*. Therefore, if $|\nabla\eta|\neq 0$, equations (A8) and (A9) can be recast in the following form:

$$\text{(azimuthal field equation)}\quad \frac{B_\phi}{\rho A'}-V_\phi=\varpi\frac{\psi'}{A'}. \tag{A12}$$

Now, let us study the consequences of the equation of motion (eq. [4]). With equation (5), the left-hand side can be written as $\nabla(V^2/2+\int dp/\rho+\Phi)$. The ϕ component is $-(V_p/\varpi)\cdot\nabla(\varpi V_\phi)+(B_p/4\pi\rho\varpi)\cdot\nabla(\varpi B_\phi)=(V_p/\varpi)\cdot\nabla[-\varpi V_\phi+(A'\varpi B_\phi/4\pi)]=0$, so that the following integral of the motion exists:

$$\text{(angular momentum)}\quad \varpi V_\phi-\frac{1}{4\pi}A'\varpi B_\phi=L(\eta), \tag{A13}$$

where $L(\eta)$, the total (including the contribution from the field) angular momentum per unit mass of outflowing material, is constant along a streamline. Solving equations (A12) and (A13) for B_ϕ, V_ϕ gives

$$B_\phi=\varpi\rho A'\left[\frac{L/\varpi^2+\psi'/A'}{1-M_A^{-2}}\right], \tag{A14}$$

$$V_\phi=\varpi\left[\frac{L/\varpi^2+M_A^{-2}(\psi'/A')}{1-M_A^{-2}}\right], \tag{A15}$$

where

$$M_A^{-2}\equiv\frac{\rho A'^2}{4\pi}=\frac{\mathbf{B}_p^2/8\pi}{\rho\mathbf{V}_p^2/2}, \tag{A16}$$

and M_A can be identified as the poloidal Alfvénic Mach number.

Two more equations need to be derived from the equation of motion. Along a streamline, $\boldsymbol{V}_p\cdot[\boldsymbol{V}\times(\nabla\times\boldsymbol{V})-\boldsymbol{B}\times(\nabla\times\boldsymbol{B})/4\pi\rho]=\boldsymbol{V}_p\cdot\nabla(\varpi B_\phi)[V_\phi A'/4\pi\varpi-B_\phi/4\pi\varpi\rho]=-\boldsymbol{V}_p\cdot\nabla(\varpi B_\phi\psi'/4\pi)$. Hence, the energy integral has the form

$$\text{(Bernoulli's equation)}\quad \frac{\mathrm{V}_p^2+\mathrm{V}_\phi^2}{2}+\int\frac{\mathrm{dp}}{\rho}+\Phi+\frac{\varpi\mathrm{B}_\phi\psi'}{4\pi}=\mathrm{E}(\eta), \tag{A17}$$

where $E(\eta)$, the total energy per unit mass of the outflowing material, is constant along a streamline. The magnetic term is $\boldsymbol{S}\cdot\hat{\boldsymbol{p}}/\rho V_p$, where $\boldsymbol{S}$ is the Poynting vector and $\hat{\boldsymbol{p}}\equiv \boldsymbol{V}_p/V_p$. Along a direction transverse to the streamlines, the final equation can be obtained by taking the dot product of $\nabla\eta$ with equation (4). With the help of equations (A12), (A13), and (A17), the left-hand side of the resulting equation can be expressed as $\nabla\eta\cdot\nabla(E-\varpi B_\phi\psi'/4\pi)=(\nabla\eta)^2E'-(\nabla\eta)^2\psi''\varpi B_\phi/4\pi-\psi'(\nabla\eta)\cdot\nabla(\varpi B_\phi/4\pi)$. Using equations (A3)–(A6) for the right-hand side, one finds ultimately the following equation:

$$\text{(transverse equation)}\ E'-\psi''\frac{\varpi B_\phi}{4\pi}-\frac{L'V_\phi}{\varpi}-A''\frac{\varpi B_\phi}{4\pi}\frac{V_\phi}{\varpi}$$
$$=\frac{1}{\varpi\rho}\left[\frac{\partial}{\partial z}\left(\frac{1}{\varpi\rho}\frac{\partial\eta}{\partial z}\right)+\frac{\partial}{\partial\varpi}\left(\frac{1}{\varpi\rho}\frac{\partial\eta}{\partial\varpi}\right)\right]-\frac{A'}{4\pi\varpi\rho}\left[\frac{\partial}{\partial z}\left(\frac{A'}{\varpi}\frac{\partial\eta}{\partial z}\right)+\frac{\partial}{\partial\varpi}\left(\frac{A'}{\varpi}\frac{\partial\eta}{\partial\varpi}\right)\right]. \tag{A18}$$

When equations (A14) and (A15) are substituted for B_ϕ and V_ϕ, equations (A17) and (A18) are two equations for $\eta(\varpi, z)$ and $\rho(\varpi, z)$. In principle, this system of equations can be solved once $A(\eta)$, $\psi(\eta)$, $l(\eta)$, and $E(\eta)$ are specified. In practice, it is obvious that equation (A18) is very difficult to solve without additional simplification.

If ψ', A', and E' are assumed constants (a simple, nontrivial choice) and all variables are assumed to be separable in ϖ and z, then inspection of equations (A14) and (A15) suggests trying ($\propto$ sign implies a multiplicative function of z) $V_\phi\propto\varpi$, $B_\phi\propto\varpi$, $L\propto\varpi^2$, and ρ independent of ϖ. These choices are consistent with the definitions of η and A (eqs. [A3]–[A6]) if $\eta(\varpi, z)\equiv-\rho(V_z/2)\varpi^2$ and V_z depends only on z. Substituting these dependencies into equations (A14), (A15), and (A18), one finds that the variable ϖ can be cancelled from these equations, and thus equation (A18) can be transformed to an ordinary differential equation in z. However, matters are not so simple for Bernoulli's equation since, as required by equation (A4), V_z is independent of ϖ while V_ϕ, V_ϖ, and B_ϕ are proportional to ϖ. Equation (A17) is necessarily split into two parts: one part has only z dependence and the other part has ϖ^2 as well as z dependence. To separate the independent variables ϖ and z in the systems, it is necessary that these two parts should be satisfied independently. The problem would then be overdetermined. To avoid this impasse, we approximate by retaining only the ϖ-independent part of Bernoulli's equation and so ignore the ϖ^2 dependent terms. This procedure is a good approximation if the flow is highly collimated along the z-direction (paraxial flow) and if the magnetic energy is always much less than the sum of the kinetic and internal energies. This is made more explicit in the text and allows us to impose only transverse self-similarity (z dependencies are unconstrained).

To make the physics of our particular solution more apparent, we return in § II from the stream functions to a more familiar set of variables. Equations (6), (7), (11), and (13) follow directly from (A11), (A14), (A15), and (A16), respectively, if we set

$$\Omega(\eta)=-\psi'/A'. \tag{A19}$$

The quantity is readily identified with $\hat{\boldsymbol{\phi}}\cdot[\boldsymbol{E}\times\boldsymbol{B}]/(\boldsymbol{B}^2\varpi)$, the angular velocity associated with the ϕ component of the drift velocity, perpendicular to $\boldsymbol{B}$, and is a constant in our particular self-similar model.

Equation (A17) is equation (12), equation (9) is the continuity equation, equation (8) is the z component of (1), while equation (10) is the radial component of (4). This latter can be easily verified to follow from equations (A17) and (A18) by multiplying (A18) by $\partial\eta/\partial\varpi$, and then using (A17) and $\partial/\partial\varpi\equiv(\partial\eta/\partial\varpi)\,d/d\eta$. It is of course the cut perpendicular to the axis rather than that perpendicular to $\boldsymbol{B}$.

APPENDIX B

ANALYTICAL APPROXIMATIONS IN THE OUTER JET REGION

In the outer jet region, as $M_A{}^{-2}$, F_c, $F_{\varpi z}\approx 0$, and $\mu_z\approx\mu_{z\infty}$, the development of the jet is described by the following single differential equation:

$$\mu_\infty{}^2\xi''=\frac{2}{\xi}(P-F_{\phi\phi}). \tag{B1}$$

As $\tau\to(\mu_\infty\xi^2)^{1-\gamma}$, and equation (32) holds,

$$P\approx\frac{1}{\gamma}(\mu_\infty\xi^2)^{-(\gamma-1)}\left[1-\gamma C_e f(\lambda)(\mu_\infty\xi^2)^{\gamma}\right] \tag{B2}$$

and

$$F_{\phi\phi}\approx\mu_\infty{}^2\epsilon_B. \tag{B3}$$

Notice that the only place where λ appears explicitly is through $f(\lambda)$. If $\gamma C_e f(\lambda)$ is approximately a constant, f_e (may be zero), in some region, then in this region a first integral of equation (B1) can be obtained as

$$(\xi')^2=4\epsilon_B\ln\left(\frac{\xi_m}{\xi}\right)+\frac{2}{\gamma}\mu_\infty{}^{-(\gamma+1)}\left[\frac{1}{(\gamma-1)}(\xi_m{}^{-2(\gamma-1)}-\xi^{-2(\gamma-1)}\right.$$
$$\left.+f_e\mu_\infty{}^\gamma(\xi_m{}^2-\xi^2))\right], \tag{B4}$$

in which ξ_m is the maximum value of ξ attained at the antinodes of the oscillations. The existence of ξ_m is obvious if either of ϵ_B or f_e is not equal to zero. When the internal pressure term is nonzero, there is also a minimum radius provided that $\gamma>1$. Thus, in general, the beam performs bounded oscillations and is confined.

There are some useful relations between geometrical (observable) properties of the jet and the physical parameters that follow from (B4) and (B1). Thus, as $\xi''=0$ at the turning radius ξ_t, (B1) yields

$$f_e=\mu_\infty{}^{-\gamma}\xi_t{}^{-2\gamma}-\frac{\gamma\mu_\infty\epsilon_B}{\xi_t{}^2}=\left(0.273\xi_t{}^{-8/3}-\frac{3.53\epsilon_B}{\xi_t{}^2},\gamma=\frac{4}{3}\right). \tag{B5}$$

As $f_e\geq 0$, we may observe immediately that

$$\epsilon_B\leq\frac{\mu_\infty{}^{-(\gamma+1)}}{\gamma}\xi_t{}^{-2(\gamma-1)}=(0.077\xi_t{}^{-2/3}), \tag{B6}$$

where the equality holds for zero external pressure.

Using (B4) at ξ_t, substituting (B5), and neglecting terms like $(\xi_t/\xi_m)^{2(\gamma-1)}$ and $(\xi_t/\xi_m)^2$ compared to unity, we obtain

$$\xi_t\approx\left[\frac{2}{\gamma\mu_\infty{}^{(\gamma+1)}}\right]^{1/2(\gamma-1)}\left[\frac{\xi_m^2/\xi_t{}^2-\gamma/(\gamma-1)}{\xi_t'^2+2\epsilon_B\xi_m{}^2/\xi_t{}^2-4\epsilon_B\ln(\xi_m/\xi_t)}\right]^{1/2(\gamma-1)}. \tag{B7}$$

On setting $\gamma=4/3$, this becomes

$$\xi_t\approx(0.061)\left[\frac{(\xi_m/\xi_t)^2-4}{(\xi_t')^2+2\epsilon_B\xi_m{}^2/\xi_t{}^2-4\epsilon_B\ln(\xi_m/\xi_t)}\right]^{3/2}. \tag{B8}$$

The right-hand sides of these latter two equations are scale independent (i.e., independent of R_s), and therefore they provide a relation between ϵ_B and $\xi_t(R_s)$ when R_m, R_t, and $(dR/dz)_t$ are observed.

Another relation follows from (B4) applied at the minimum radius, $\xi_{\min}(\equiv\xi_n)$ at the nodes where $\xi'=0$ as (with similar approximations to those of [B7])

$$0\approx4\epsilon_B\ln\left(\frac{\xi_m}{\xi_n}\right)-\frac{2\mu_\infty{}^{-(\gamma+1)}}{\gamma(\gamma-1)}\left\{\xi_n{}^{-2(\gamma-1)}-(\gamma-1)\xi_m{}^2\left[\xi_t{}^{-2\gamma}-\frac{\gamma\mu_\infty{}^{\gamma+1}\epsilon_B}{\xi_t{}^2}\right]\right\}. \tag{B9}$$

If R_n is also observed, then this relation provides a second relation between R_s and ϵ_B to be used with (B7). When $\gamma=4/3$, (B9) becomes

$$0\approx4\epsilon_B\ln\left(\frac{\xi_m}{\xi_n}\right)-0.465\xi_n{}^{-2/3}+0.155\xi_m{}^2\left[\xi_t{}^{-8/3}-\frac{12.9\epsilon_B}{\xi_t{}^2}\right]. \tag{B10}$$

The preceding analysis is particularly simple if either $f_e=0$ (pure magnetic pinching) or $\epsilon_B=0$ (external pressure pinching). When $\epsilon_B=0$, (B7) gives an immediate value for $\xi_t(R_s)$ when R_m, R_t, and $(dR/dz)_t$ are observed. Then

(B5) provides an estimate of the external pressure "plateau" required ($f_e = p_e/p_{js}$). Equation (B9) (with $\epsilon_B = 0$) then provides either a prediction for ξ_n or a consistency check if R_n is observed.

Should $f_e = 0$, then the analog of (B7) becomes

$$\xi_t = \left[\frac{2}{\gamma(\gamma-1)\mu_\infty{}^{(\gamma+1)}}\right]^{1/2(\gamma-1)} \Big/ \left[4\epsilon_B \ln\left(\frac{\xi_m}{\xi_t}\right) - (\xi_t')^2\right]^{1/2(\gamma-1)}$$

$$= 0.317/\left[4\epsilon_B \ln(\xi_m/\xi_t) - (\xi_t')^2\right]^{3/2}, \quad \gamma = 4/3. \tag{B11}$$

Moreover (B9) yields

$$\xi_n = \left[\frac{2\mu_\infty{}^{-(\gamma+1)}}{\gamma(\gamma-1)}\right]^{1/2(\gamma-1)} \Big/ \left[4\epsilon_B \ln\left(\frac{\xi_m}{\xi_n}\right)\right]^{1/2(\gamma-1)}$$

$$= 0.317/\left[4\epsilon_B \ln\left(\frac{\xi_m}{\xi_n}\right)\right]^{3/2}, \quad \gamma = 4/3, \tag{B12}$$

and the equality holds in (B6). When R_t, R_n, R_m, and $(dR/dz)_t$ are observed, two of equations (B11), (B12), and (B6) may be solved for ϵ_B, R_s, and the third is a consistency check.

We wish to urge caution in the use of these latter formulae as they are strictly asymptotic results. They do not agree well with the numerical results in Table 3 [which are for $f(\lambda) \neq 0$] showing that even an asymptotically vanishing external pressure has significant effects as finite λ. We have verified that these formulae become valid as $\lambda_t \to \infty$, however. In particular, formula (B8) becomes

$$\xi_t \simeq 0.0216\epsilon_B{}^{-3/2};$$

and we do find numerical agreement with this result asymptotically (see Gaussian cases in Table 3).

When in this last case the internal pressure is also negligible, ξ_m/ξ_n is large. In this case the formal zero pressure limit in (B4) ($f_e = 0$: $\gamma \to \infty$) may be integrated to yield the scale over which ξ will collapse from ξ_m to ξ_n (~ 0 in this limit). We find $\Delta\lambda \equiv \lambda_m - \lambda_n = \xi_m \sqrt{\pi/(4\epsilon_B)}$, and hence

$$\epsilon_B = \frac{\pi}{4}\frac{\xi_m{}^2}{(\Delta\lambda)^2} \equiv \frac{\pi}{4}\frac{R_m{}^2}{(z_m - z_n)^2}. \tag{B13}$$

This yields ϵ_B directly and replaces (B11) and (B6). Equation (B12) will still give a rough estimate of ξ_n, or a consistency check. Equation (46) provides a restriction on R_s, M_{As} if R_1 is observed.

We would like finally to consider briefly projection effects. The projected radii required will be close to their true values in an axisymmetric jet, while the projected $\Delta\lambda$ would be $(\Delta\lambda)_{\text{true}} \cos\Delta$ if the axis of the jet makes the angle Δ with the plane of the sky. Thus the derivative required above, $(dR/dz)_t$, would be

$$(dR/dz)_{\text{true}} = (dR/dz)_{\text{proj}} \cos\Delta,$$

and

$$(\epsilon_B)_{\text{true}} = (\epsilon_B)_{\text{proj}} \cos^2\Delta. \tag{B14}$$

Moreover, from equation (46) we infer ($\xi_1 \propto \epsilon_B{}^{-1/2}$)

$$(\xi_1)_{\text{true}} \approx \cos^{-1}\Delta(\xi_1)_{\text{proj}},$$

and therefore

$$(R_s)_{\text{true}} \approx (R_s)_{\text{proj}} \cos\Delta \equiv \frac{(R_1)_{\text{proj}}}{(\xi_1)_{\text{proj}}} \cos\Delta. \tag{B15}$$

REFERENCES

Begelman, M. C., Rees, M. J., and Blandford, R. D. 1979, *Nature*, **279**, 770.
Benford, G. 1978, *M.N.R.A.S.*, **183**, 29.
Birkhoff, G., and Zarontonello, E. H. 1957, *Jets, Wakes and Cavitons* (New York: Academic).
Blake, G. M. 1972, *M.N.R.A.S.*, **156**, 67.
Blandford, R. D. 1976, *M.N.R.A.S.*, **176**, 465.
Blandford, R. D., and Rees, M. J. 1974, *M.N.R.A.S.*, **169**, 395 (BR).
Bridle, A. H., Davis, M. M., Fomalont, E. B., Willis, A. G., and Strom, R. G. 1979, *Ap. J.* (*Letters*), **228**, L9.
Bridle, A. H., Davis, M. M., Meloy, D. A., Fomalont, E. B., Willis, A. G., and Strom, R. G. 1976, *Nature*, **262**, 179.
Burch, S. F. 1977, *M.N.R.A.S.*, **181**, 599.
Chan, K. L., Chau, W. Y., and Henriksen, R. N. 1980, *Ap. J.*, in press.
Fomalont, E. B., Bridle, A. H., Willis, A. G., and Perley, R. A. 1980, *Ap. J.*, in press.
Goldreich, P., and Julian, W. H. 1970, *Ap. J.*, **160**, 971.
Henriksen, R. N., and Rayburn, D. R. 1971, *M.N.R.A.S.*, **152**, 323.
Landau, L. D., and Lifshitz, E. M. 1959, *Fluid Mechanics* (London: Pergamon Press).
Longair, M. S., Ryle, M., and Scheuer, P. A. G. 1973, *M.N.R.A.S.*, **164**, 243.
Lovelace, R. V. E. 1976, *Nature*, **262**, 649.
Mestel, L. 1968, *M.N.R.A.S.*, **138**, 359.
Michel, F. C. 1969, *Ap. J.*, **158**, 727.
Pacholczyk, A. G. 1970, *Radio Astrophysics* (San Francisco: Freeman).
Perley, R. A., Willis, A. G., and Scott, J. S. 1979, *Nature*, **281**, 437.
Readhead, A. C. S., Cohen, M. H., and Blandford, R. D. 1978, *Nature*, **272**, 131.
Rees, M. J. 1971, *Nature*, **229**, 312 and 510.
Scheuer, P. A. G. 1974, *M.N.R.A.S.*, **166**, 513.
Waggett, P. C., Warner, P. J., and Baldwin, J. E. 1977, *M.N.R.A.S.*, **181**, 465.
Weber, E. J., and Davis, L., Jr. 1967, *Ap. J.*, **148**, 217.
Wiita, P. J. 1978, *Ap. J.*, **221**, 41.

K. L. CHAN: Applied Research and Systems, 1998 Generals Highway, Annapolis, MD 21401

R. N. HENRIKSEN: Astronomy Group, Queen's University at Kingston, Kingston, Ontario, K7L 3N6, Canada